Structure and Conservation of the Periplasmic Targeting Factor Tic22 Protein from Plants and Cyanobacteria*[S]

Joanna Tripp[‡1], **Alexander Hahn**[‡§1], **Patrick Koenig**[¶2], **Nadine Flinner**[‡||], **Daniela Bublak**[‡], **Eva M. Brouwer**[‡],
Franziska Ertel[‡3], **Oliver Mirus**[‡], **Irmgard Sinning**[¶], **Ivo Tews**[¶4,5], and **Enrico Schleiff**[‡§||5,6]

From the ‡Department of Biosciences, ||Center of Membrane Proteomics, §Cluster of Excellence Frankfurt, Goethe University, 60438
Frankfurt, Germany and ¶Heidelberg University Biochemistry Center (BZH), 69120 Heidelberg, Germany

Background: Although Tic22 is involved in protein import into chloroplasts, the function in cyanobacteria is unknown.
Results: Cyanobacterial Tic22 is required for OM biogenesis, shares structural features with chaperones, and can be substituted by plant Tic22.
Conclusion: Tic22, involved in outer membrane biogenesis, is functionally conserved in cyanobacteria and plants.
Significance: The findings are important for the understanding of periplasmic protein transport.

Mitochondria and chloroplasts are of endosymbiotic origin. Their integration into cells entailed the development of protein translocons, partially by recycling bacterial proteins. We demonstrate the evolutionary conservation of the translocon component Tic22 between cyanobacteria and chloroplasts. Tic22 in *Anabaena* sp. PCC 7120 is essential. The protein is localized in the thylakoids and in the periplasm and can be functionally replaced by a plant orthologue. Tic22 physically interacts with the outer envelope biogenesis factor Omp85 *in vitro* and *in vivo*, the latter exemplified by immunoprecipitation after chemical cross-linking. The physical interaction together with the phenotype of a *tic22* mutant comparable with the one of the *omp85* mutant indicates a concerted function of both proteins. The three-dimensional structure allows the definition of conserved hydrophobic pockets comparable with those of ClpS or BamB. The results presented suggest a function of Tic22 in outer membrane biogenesis.

Mitochondria and chloroplasts originated from bacteria by evolutionary adaptation after inheritance by the host cell (1, 2), with the latter enforcing the development of machines for translocation of cytosolically synthesized proteins into these organelles. These machines originated in parts from bacterial proteins forming a minimal system of only few components, whereas additional factors were added in the course of evolution to enhance specificity and/or kinetics of translocation (3, 4). Distinct membrane-localized complexes are responsible for sorting of proteins into the different compartments of the organelles (5–7). The translocons on the outer or inner chloroplast envelope (TOC/TIC) are required for the transfer of preproteins into the stroma (6, 7), and transfer of preproteins across the intermembrane space is assisted by Tic22 (8–10).

Albeit bacterial homologues to several mitochondrial and chloroplast translocon components were identified (3, 4, 11), a functional relationship is only established for Toc75-III, Sam50, and the bacterial Omp85 (3, 4, 11, 12). The bacterial Omp85 is involved in membrane insertion of bacterial OMPs (13), which is conserved for Sam50 and most likely for Toc75-V/Oep80, whereas Toc75-III is involved in the translocation of proteins across the membrane (14). By this, the central component of the eukaryotic translocation machines appears to be inherited from bacteria.

Omp85 proteins N-terminally contain a repeat of polypeptide transport-associated (POTRA) segments, which is called a POTRA domain, and C-terminally contain a membrane-embedded β-barrel (14 and 15 and references therein). The N-terminal POTRA[7] domain of the protein from *Anabaena* sp. PCC 7120 (*Anabaena* sp. hereafter) encoded by alr2269 is composed of three POTRA elements (*e.g.* 16 and 17) and is discussed to represent some kind of a receptor domain. The precise function of the POTRA domain, however, is not yet fully explored and might differ for the Omp85 proteins from different bacteria (14, 15).

Remarkably, the periplasmic Tic22 also is found in both cyanobacteria and plastids (see Fig. 1 and supplemental Fig. S1) (9, 18, 19). In plastids, it is the only known soluble intermembrane space component interacting with the translocation complexes

TABLE 1

Plasmids generated in this study

Plasmid	Resistance[a]	Source plasmid	Genotype
p*ana*Tic22	Amp[R]	pET21b[b]	
p*ana*OMP85-POTRA[c]	Amp[R]	Topo-TrcHis2[d]	
pJT13	Sp[R]/Sm[R]	pCSEL24[e]	pCSEL24 (P$_{alr0114}$/GFP)
pJT14	Sp[R]/Sm[R]	pRL271[f]	pRL271 (orf$_{alr0114}$ bp 1–404/Sp[R]/Sm[R]/423–825)
pALH1	Nm[R]	pRL271	pRL271 *sacB*::Nm[R]
pALH2	Nm[R]	pALH1	pALH1 (P$_{petJ}$/*alr0114*)
pALH3	Nm[R]	pALH1	pALH1 (P$_{petJ}$/*alr0114* D213R)
pALH4	Nm[R]	pALH1	pALH1 (P$_{petJ}$/*alr0114* I219R)
pALH5	Nm[R]	pALH1	pALH1 (P$_{petJ}$/*alr0114* F136G)
pALH6	Nm[R]	pALH1	pALH1 (P$_{petJ}$/*ssalr0114-at*Tic22)

[a] Amp[R], ampicilin; Sp, spectinomycin; Sm, streptomycin; Nm, neomycin.
[b] Novagen.
[c] Ref. 16.
[d] Invitrogen.
[e] Ref. 56.
[f] Ref. 57.

TABLE 2

Used and generated strains

Sp (spectinomycin), Sm (streptomycin), Nm (neomycin) AFS (*Anabaena* sp., mutant created in Frankfurt by a member of the Schleiff group), AFS-I (AFS with an insertion in the gene specified), and AFS-PDGF (promoter downstream GFP fusion).

Strain	Resistance	Genotype	Relevant properties	References
AFS-I-*tic22*	Sp[R]/Sm[R]	*alr0114*::pJT14	Gene interruption	This study
AFS-I-*alr0075*	Sp[R]/Sm[R]	*alr0075*::Sp[R]/Sm[R]	Gene interruption	Ref. 23
AFS-I-*alr2269*	Sp[R]/Sm[R]	*alr2269*::Sp[R]/Sm[R]	Gene interruption	Ref. 23
AFS-I-*alr2270*	Sp[R]/Sm[R]	*alr2270*::Sp[R]/Sm[R]	Gene interruption	Ref. 23
AFS-I-*alr4893*	Sp[R]/Sm[R]	*alr4893*::Sp[R]/Sm[R]	Gene interruption	Ref. 23
AFS-I-*alr2887*	Sp[R]/Sm[R]	*alr2887*::Sp[R]/Sm[R]	Gene interruption	Ref. 22
AFS-PDGF-*tic22*	Sp[R]/Sm[R]	nucA region::pJT13	Promoter-GFP fusion	This study
AFS-I-*tic22* petJ/*anatic22*	Sp[R]/Sm[R]/Nm[R]	*alr0114*::pJT14 pALH2	Complementation	This study
AFS-I-*tic22* petJ/D213R	Sp[R]/Sm[R]/Nm[R]	*alr0114*::pJT14 pALH3	Complementation	This study
AFS-I-*tic22* petJ/I219R	Sp[R]/Sm[R]/Nm[R]	*alr0114*::pJT14 pALH4	Complementation	This study
AFS-I-*tic22* petJ/F136G	Sp[R]/Sm[R]/Nm[R]	*alr0114*::pJT14 pALH5	Complementation	This study
AFS-I-*tic22* petJ/*at*Tic22	Sp[R]/Sm[R]/Nm[R]	*alr0114*::pJT14 pALH6	Complementation	This study

in both enve lopes (8 –10). The molecular function of cyanobacterial Tic22 is presently unclear. In *Synechocystis* sp. PCC 6803, Tic22 (Slr0924) was identified in the periplasmic proteome (19), whereas a thylakoid localization was suggested by immunoelectron microscopy (18).

Here, we show that *ana*Tic22 (Alr0114) from *Anabaena* sp. is soluble and localized in both the thylakoids and periplasm. *tic22* mutants show a similar phenotype as *omp85* mutants and a physical interaction between *ana*Tic22 and *ana*Omp85 was observed. The crystallographic three-dimensional structure of *ana*Tic22 revealed a novel fold with hydrophobic surface pockets. Similar pockets binding to aromatic amino acids were observed for ClpS (20) and BamB (21), suggesting that Tic22 recognizes the C-terminal OMP signal containing an aromatic amino acid (13). On the one hand, this provides insights into the periplasmic protein transport system in cyanobacteria; on the other hand, Tic22 provides a second example for functional conservation between bacterial and chloroplast proteins in protein translocation.

EXPERIMENTAL PROCEDURES

Generation, Growth, and handling of Anabaena Strains— Plasmids (Table 1) or *Anabaena* strains (Table 2) were described or generated as established (22–24). For cloning of *alr0114* (*anatic22*), PCR was performed on genomic DNA of *Anabaena* sp. (supplemental Table S1) (23). For complementation, the ORF of *anatic22* was fused to the copper-regulated promoter petJ and cloned into pALH1, a derivate of pRL271 where Cm[R]/Em[R] and the *SacB* gene were replaced by the neo-

mycin resistance cassette C.K1. Mutants of *anatic22* were generated by site-directed mutagenesis. The construct of *at*Tic22-IV was produced by RT-PCR, and the ORF was fused to the promoter of petJ and the coding sequence for Alr0114 signal peptide determined by SignalP (25). Cultures of *Anabaena* were grown in BG11 (26) supplemented as described (23, 24). The analysis of GFP fluorescence and *Anabaena* sp. fractionation was performed as described (16, 27).

Heterologous Expression and Antibody Production—For heterologous expression of *alr0114* and subsequent protein purification, a fragment encoding amino acids 32–274 was amplified with primers containing restriction sites NdeI and XhoI (supplemental Table S1), and subsequently cloned into pET21b digested with NdeI and XhoI. For inactivation of *alr0114*, two fragments of ~400 bp encoding the N- and C-terminal half of *alr0114* were amplified using the primers indicated in supplemental Table S1, which include XhoI/HindIII and HindIII/PstI restriction sites, respectively. Following cleavage with these restriction enzymes, the generated PCR fragments were cloned into pRL271 cut with XhoI and PstI. Subsequently, a fragment containing the Sp/Sm resistance cassette was produced by cleavage of pCSEL24 with HindIII and inserted between the two fragments. For generation of pJT13 carrying the translational fusion of the *alr0114* promoter with GFP, a DNA fragment of ~800 bp of the upstream region and the region encoding the first eight amino acids of the ORF of *alr0114* and were amplified by PCR with the primers indicated in supplemental Table S1, containing PstI and AatII restriction sites. The ORF of

GFP was amplified using primers containing the restriction sites AatII and EcoRI. The generated PCR fragments were cut with PstI/AatII and AatII/EcoRI, respectively, and inserted into pCSEL24 digested with PstI and EcoRI.

The coding region of *anatic22* without signal sequence was cloned into pET21b (Novagen). Recombinant *ana*Tic22 was expressed in *Escherichia coli* BL21(DE3) induced by addition of 1 mM isopropyl 1-thio-β-D-galactopyranoside at $A_{600} = 0.6$ and cells harvested 4 h after induction at 37 °C. Cell lysis and protein purification via nickel-NTA chromatography (Qiagen) was performed according to the manufacturer's instructions. Antibodies against *ana*Tic22 were produced by Pineda antibody service (Berlin, Germany).

Electron Microscopy—Preparation of *Anabaena* sp. for EM was done according to (28) with the following adaptations. 50 ml of *Anabaena* cell culture $A_{750} = 1.5$ was pelleted by centrifugation at $2,000 \times g$, collected in 20 ml of fixate solution (BG11 + 2.5% glutaraldehyde) and incubated for 1 h at room temperature. Afterward, cells were washed two times with wash buffer (50 mM Na-cacodylat, pH 7.2, 0.4 M sucrose), and collected in 1 ml of wash buffer. Cells were mixed with 2 volumes of 2% OsO_4 solution and incubated for 2.5 h at room temperature. Afterward, cells were washed two times in wash buffer. Subsequently, cells were dehydrated by incubation for 20 min in 30, 50, 70, 80, 90, and $2 \times 100\%$ ethanol and twice 20 min in propylenoxid. Afterward, cells were collected in a 1:1 mixture of propylenoxid and araldite and incubated overnight at room temperature. Cells were finally embedded in araldite and incubated overnight at 48 °C.

Pulldown Analysis of Interacting Proteins—The *ana*Omp85-POTRA (residues 161 to 470) with C-terminal His tag (*ana*Omp85-POTRA-HIS) was expressed and purified as in (16, 17). Protein in 150 mM NaCl, 20 mM NaP$_i$, pH 7.6 was bound to Ni-NTA. The supernatant of *Anabaena* cells in 5 mM Hepes, pH 8.0, 1 mM PMSF after opening by French pressing was incubated with the affinity matrix for 30 min. The matrix was washed (20 mM Hepes, pH 8.0, 150 mM KCl), and proteins were eluted (20 mM Hepes, pH 8.0, 500 mM NaCl). The efficiency of *ana*Omp85 binding was controlled by elution with 500 mM imidazole. The proteins were identified by mass spectrometric analysis (27).

In Vitro Analysis of anaTic22-POTRA Interaction—100 μg of purified protein (total) in 100 μl of 25 mM Hepes, pH 7.0, 250 mM NaCl, 500 mM imidazole was incubated with 0.023% glutaraldehyde for 5 min at 37 °C. The reaction was stopped by addition of 100 mM Tris HCl, pH 8.0. 10% of the reaction was separated using a 10% SDS-PAGE followed by Coomassie Blue staining.

In Vivo Analysis of anaTic22-POTRA Interaction—50 ml of *Anabaena* culture was harvested by centrifugation at $4,000 \times g$, 5 min at 22 °C. The pellet was washed with 10 ml of PBS buffer and resuspended in PBS containing 10 ml of 1% (v/v) formaldehyde for 30 min. The reaction was stopped by resuspension in PBS supplemented with 0.25 M glycine. Cells were subsequently lysed by two French press cycles at 1,200 psi. The membrane was recovered by centrifugation at $87,000 \times g$ and subsequently solubilized by incubation with 1.5% digitonin in PBS for 30 min on ice. The solution was cleared by centrifugation and diluted by addition of PBS to 0.3% digitonin (final concentration). Antibodies raised against *ana*Omp85 were added. After 1 h of incubation, the solution was incubated overnight at 4 °C with 25 μl of protein A-Sepharose. The matrix was washed four times with PBS with 0.3% digitonin, and bound proteins were eluted with 50 μl of 2$\times$ SDS-loading buffer. 15 μl were subjected to 10% SDS-PAGE. The cross-linked product was excised from the gel, boiled for 30 min, and subjected to a 12% SDS-PAGE followed by blotting to nitrocellulose and immunodecoration with *ana*Tic22 antibodies.

Crystal Structure Determination of anaTic22—*anatic22* ORF (*alr0114*) from *Anabaena* sp. was cloned into pET21b (Novagen) omitting the signal sequence. *E. coli* BL21(DE3) cells were transformed and grown at 37 °C in LB medium, and expression was induced by addition of 1 mM isopropyl 1-thio-β-D-galactopyranoside at $A_{600} = 0.6$ and grown for 3 h. Cells were resuspended in buffer A (50 mM Tris-HCl, pH 7.5, containing 300 mM NaCl and 10 mM imidazole) and lysed using an M110 microfluidizer at 15,000 p.s.i./100 megapascal (Microfluidics). The cell lysate was cleared by centrifugation, supernatant was loaded on a HisTrap Ni-affinity column (GE Healthcare), and protein was eluted (buffer A with 250 mM imidazole). Size exclusion chromatography (S75 26/60 column, GE Healthcare) in 20 mM Hepes, pH 7.5, containing 200 mM NaCl was used for final purification. Crystallization was performed at 20 °C, using sitting-drop vapor diffusion with 1-μl drop size. Crystals were obtained from 1 M sodium citrate, 0.1 M CHES, pH 9.5, harvested in cryoprotectant buffer, and flash-frozen in liquid nitrogen.

Seleno-methionine-labeled *ana*Tic22 was obtained using a metabolic inhibition expression protocol (29) and crystallized from 1 M sodium citrate, 0.15 mM $MgCl_2$, 0.1 M CHES, pH 9.5. Data were collected at the European Synchrotron Radiation Facility. Data were integrated and scaled with HKL software (HKL Research, Inc.) and processed by standard procedures. Data reduction, free R assignment, and data manipulation were carried out with the CCP4 suite. The structure was determined by multiple anomalous dispersion phasing using SOLVE (30). Iterative model building and refinement were carried out with Coot (31) and REFMAC5 (32) and cycled with ARP (33). The structure quality was accessed using PROCHECK (34).

RESULTS

anaTic22 Is Expressed in Both Cell Types and Localized in Periplasm and Thylakoids—Several TOC or TIC components share a common ancestor with proteins from cyanobacteria such as *Anabaena* sp. PCC 7120 (*Anabaena* sp. hereafter; Fig. 1). We analyzed Tic22, which is found in both cyanobacteria and plastids (supplemental Fig. S1). For the cyanobacterial Tic22 in *Synechocystis* sp. PCC 6803 (Slr0924), a periplasmic and thylakoid localization was suggested. We confirmed both results. By using a promoter GFP fusion as established previously (strain AFS-PDGF-*tic22*, Tables 1 and 2 and supplemental Table S1) (Fig. 2*A* and see Fig. 3) (22–24), we show that the promoter is active in all cells, including heterocysts (Fig. 2*A*, *white triangle*). The subcellular localization of *ana*Tic22 was determined by fractionation of *Anabaena* sp. into soluble, cell wall-integrated and -associated, as well as thylakoid compo-
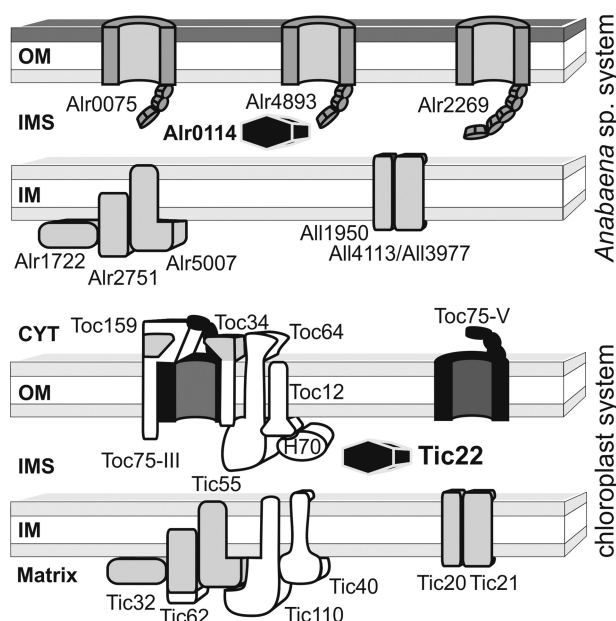
FIGURE 1. **Evolutionary conservation of the chloroplast protein translocation system.** Analysis of TOC or TIC components shows that most of the identified components have homologues in *Anabaena* sp. PCC 7120 (protein name is chosen according to the gene name). Exceptions for which a homologue is not identified are shown in *white*. The functional relation between Toc75 (*black*) and the cyanobacterial Omp85 (encoded by *alr0075*, *alr4893*, *alr2269*) was demonstrated previously (4). Chloroplast proteins marked in *gray* showcases where proteins (*e.g.* Tic20, Tic21, etc.) or protein domains (Toc159; Toc34, Tic62) have possibly been recycled to a new function. The investigated Tic22 is highlighted (Alr0114; *ana*Tic22). *OM*, outer membrane; *IMS*, inner membrane space; *IM*, inner membrane; *CYT*, cytosol.
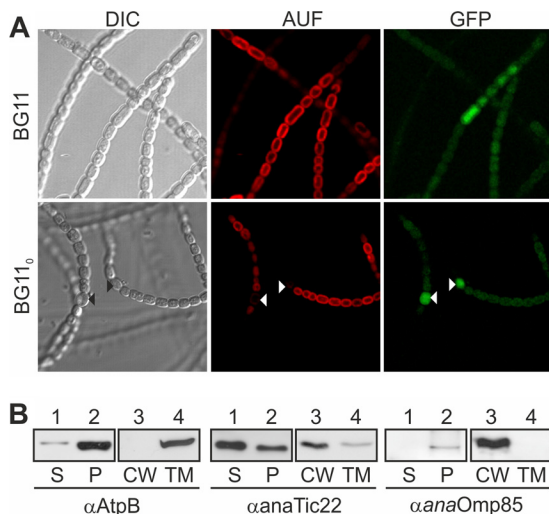

FIGURE 2. **The localization of *ana*Tic22.** *A,* light microscopy images of *Anabaena* sp. mutant strain AFS-PDGF-*tic22* (*left*) grown in BG11 (*top*) or BG11$_0$ (*bottom*), and confocal fluorescence images of the chlorophyll autofluorescence (*middle*) and GFP (*right*) are shown. *Triangles* mark heterocysts. *B, Anabaena* sp. was fractionated into soluble (*S*) and pellet fraction (*P*); the latter in cell wall (*CW*) and thylakoid membranes (*TM*). Samples were immunodecorated with indicated antibodies. *AUF*, autofluorescence, *DIC*, differential interference contrast.

nents. The fractionation was controlled by immunostaining against the thylakoid protein AtpB and the outer membrane protein Omp85 (Fig. 2*B*), which show the two fractions are not cross-contaminated. *ana*Tic22 was identified in both, the thylakoid and cell wall fraction (Fig. 2*B*), indicating a dual localization in cyanobacterial cells.

anaTic22 Performs Function in Outer Membrane Biogenesis—To analyze the function of *ana*Tic22, we generated an insertion mutant by introducing the pJT14 into the coding region of *anatic22* (Fig. 3*A* and Table 1) (AFS-I-*tic22*, I-*tic22* hereafter). The cassette was inserted at base pair 403 in the middle of the coding sequence. We were unable to fully segregate the mutant, but by PCR on genomic DNA, we confirm that most of the genomic copies contained the insertion (Fig. 3*B*, *lanes 3* and *4*). However, in I-*tic22*, the *ana*Tic22 protein content is reduced at least 10-fold as judged from immunodecoration with antibodies against *ana*Tic22 (Fig. 3*C*), which justifies the use of the mutant for further analysis.

The phenotype of I-*tic22* was compared with those of other mutants affecting OM functionality, namely mutants of Omp85 homologues (encoded by *alr0075*, *alr4893*, and *alr2269* (*anaomp85*)), the TolC-like HgdD (*alr2887*) and LpxC (*alr2270*) involved in lipid A synthesis (22, 23). All strains grow on BG11 (Fig. 3*D*, *panel 1*). On BG11$_0$, a medium without fixed nitrogen source, all strains except the mutant of *alr0075* showed reduced growth compared with a control strain (CSR10 (35)) (Fig. 3*D*, *panel 3*). With ammonium as a nitrogen source, we could further differentiate these observations, as only I-*alr2270*, I-*alr2269*, and I-*tic22* were retarded in growth (Fig. 2*B*, *panel 5*). We next investigated the growth of the mutants in the presence of lysozyme to assay OM permeability (23). For I-*alr2270*, I-*alr2269*, I-*alr2887*, and I-*tic22*, we observed an enhanced sensitivity to lysozyme at concentrations of ≥30 mM as established (Fig. 3*D*, *panels 2* and *4*).

Furthermore, the insertion mutants of *alr2269* and *anatic22* have altered outer membrane morphology as determined by electron microscopy (Fig. 3*E* and supplemental Fig. S2). Using a staining method focusing on the outer membrane structure, we observed a rather smooth outer membrane structure of wild-type cells, whereas in both mutants, the outer membrane is rippled although in I-*alr2269* to a larger extend. This difference was observed in all preparations (supplemental Fig. S2). In addition, the peptidoglycan layer seems to be rippled as well, which however might be the result of the alteration of the outer membrane morphology.

To confirm that the phenotype is indeed attributed to the mutation of *anatic22*, we analyzed whether *anatic22* and *alr0115* are transcribed on a common transcript in wild-type. We observed an overlapping transcript between *anatic22* and *alr0115*, as well as between *alr0115* and *alr0116* (Fig. 4*A*, *lanes 4* and *6*). As a consequence, both genes *alr0115* and *alr0116* are reduced in I-*tic22* as determined by RT-PCR and comparison with the transcript abundance seen in wild-type (WT, Fig. 4*B*, *lanes 1 versus 2* and *lanes 3 versus 4*). The transcript abundance of *alr0117* was only moderately affected (*lane 5 versus 6*). Thus, we complemented the mutant I-*tic22* with *anatic22* to confirm that the phenotype is specific to *ana*Tic22 depletion. Indeed, the phenotype is not attributed to a malfunction of a downstream gene as complementation with *anatic22* leads to a wild-type-like behavior with respect to the tested conditions (I-*tic22* petJ/ana*tic22*; Fig. 4*C*). These results suggest a function of cyanobacterial Tic22 in outer membrane biogenesis.

Plant and Cyanobacterial Tic22 Are Functionally Conserved—The plant Tic22, like several other TOC or TIC components,
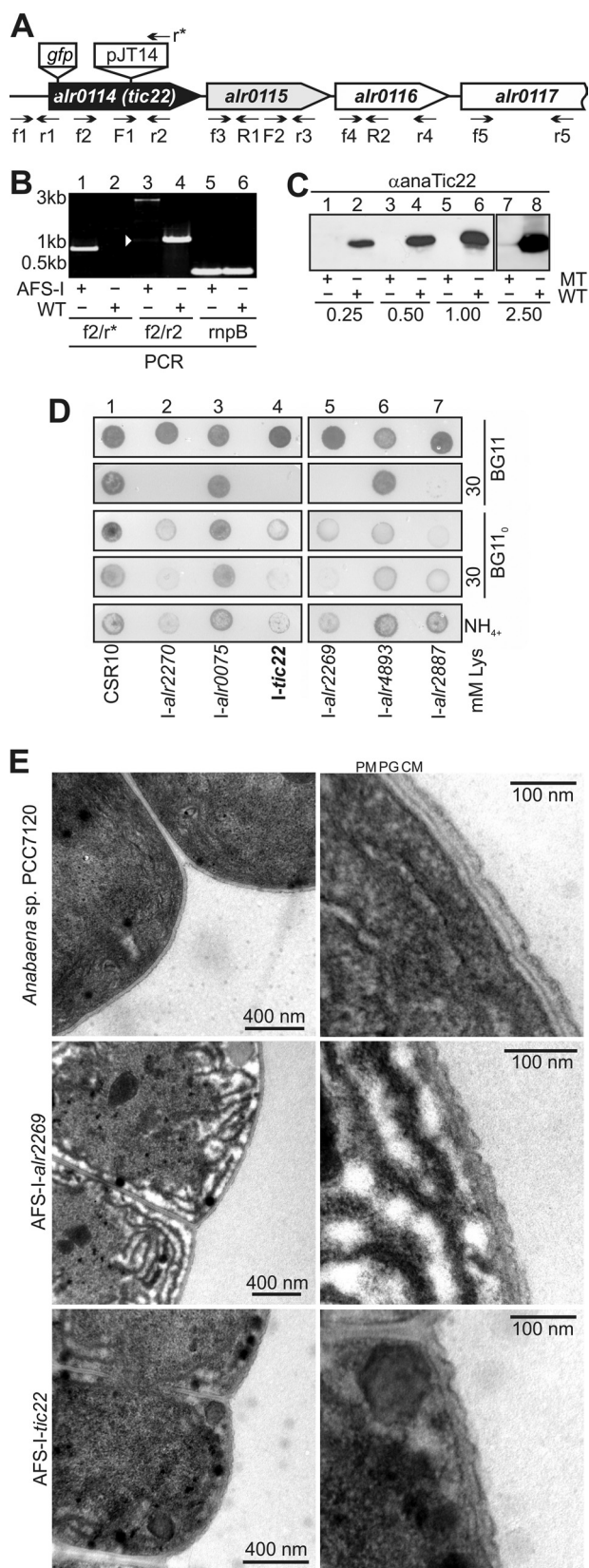
FIGURE 3. ***ana*Tic22 is involved in OM biogenesis.** *A*, the genomic structure of *ana*Tic22, including downstream encoded genes, the annealing position of the oligonucleotides, the position of GFP insertion to generate strain AFS-PDGF-*tic22* and the position of the plasmid insertion to generate strain AFS-I-*tic22* are indicated. *B*, shown is the PCR on genomic DNA isolated from AFS-I-*tic22* (AFS-I) and *Anabaena* sp. PCC 7120 (WT) using the indicated primer combinations (*lanes 1–4*). The amplification of the *rnpB* region was used as loading control. *C*, immunodecoration of cell lysates of I-*tic22* (*MT*, *lanes 1, 3, 5*) or *Anabaena* sp. (*WT*, *lanes 2, 4, 6*) at indicated protein amounts (mg) with *ana*Tic22 antibodies. Loading was controlled by Ponceau staining. *D*, 2 μl of indicated strains (2.5 mg chlorophyll ml^{-1}) were spotted on BG11 (*panels 1* and *2*), BG11$_0$ (*panels 3* and *4*), or BG11$_{NH4}$ plates (NH$_4$, *panel 5*) containing 30 mM lysozyme (*panels 2* and *4*; images after 7 days). *E*, the ultrastructure of the outer membrane of the indicated strains was analyzed by electron microscopy as described under "Experimental Procedures." Additional images are shown in supplemental Fig. S2.

shares a common ancestor with proteins from cyanobacteria (Fig. 1 and supplemental Fig. S1). To confirm orthology, we analyzed whether *at*Tic22-IV (AT4G33350) from *Arabidopsis thaliana* can complement for the *ana*Tic22 defect in I-*tic22*. To this end, the cDNA of *at*Tic22-IV was transferred into the *Anabaena* sp. *ana*tic22 mutant (I-*tic22* petJ/*at*Tic22). Indeed, the expressed protein was able to complement for the growth arrest of the mutant strain at elevated lysozyme levels. Although we observed a slightly slower growth than wild-type (Fig. 4*C*), it confirms the functional conservation of the two proteins.

Tic22 Genetically and Physically Interacts with Omp85—The results suggest a function of cyanobacterial Tic22 in outer membrane homeostasis. Prompted by this observation, we analyzed *ana*Tic22 abundance in the mutants mentioned above (Fig. 4*D*). In the mutant of *alr0075* and *hgdD*, we observed protein levels comparable with the control strain. In the other mutants, the level of *ana*Tic22 is significantly enhanced up to 5-fold (Fig. 4*D* and supplemental Fig. S3), which correlates with the observed phenotypic profile. We conclude that a disturbance of the molecular machines required for OM protein biogenesis, but not of OM in general, leads to elevated Tic22 protein levels. However, the level of *ana*Omp85 is not drastically affected in the *ana*tic22 mutant (Fig. 4*E*), whereas in the mutant affecting lipid A synthesis (I-*alr2270*) Omp85 is and its precursor (*) are slightly accumulated. On the one hand, this finding suggests that Omp85 insertion into the outer membrane can bypass the Tic22 function; on the other hand, it documents that the phenotype observed for *ana*tic22 mutants is not the result of reduced levels of *ana*Omp85.

To confirm the functional link, *ana*Tic22 and *ana*Omp85 were tested for a direct interaction. We expressed the periplasmic-exposed POTRA domains of *ana*Omp85 (*ana*Omp85-POTRA-HIS; 24), immobilized the protein on Ni^{2+}-NTA, and incubated it with soluble extract from *Anabaena* sp. We compared the elution fractions in the absence (Fig. 4*F*, *left*) or presence of *ana*Omp85-POTRA-HIS (Fig. 4*E*, *right*) and observed two small proteins specifically bound and not found in the control co-eluted with *ana*Omp85. Mass spectrometric analysis confirmed the identity of the upper band as *ana*Tic22, whereas sequencing of the according region in the control fraction did not lead to a significant detection of a protein. Although the interaction was rather weak, the periplasmic chaperone SurA and Omp85 (BamA) of *E. coli* likewise showed weak interaction that had to be stabilized by chemical cross-linking (36). To confirm the proposed interaction between *ana*Tic22 and *ana*Omp85-POTRA, we used a similar cross-linking approach (36).
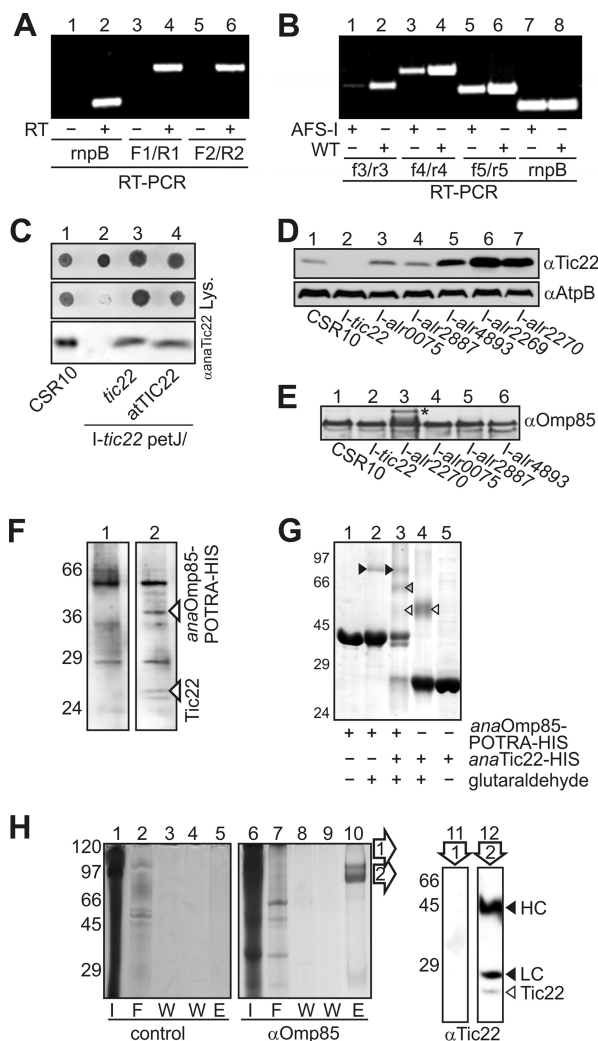
FIGURE 4. Analysis of *tic22* and *alr0115* expression in the mutant. *A*, RNA from wild-type *Anabaena* sp. PCC 7120 was isolated and either rnpB or the indicated intergenic regions amplified by RT-PCR in the presence (+) or absence of reverse transcriptase (−). Primers used are indicted in Fig. 3*A*. *B*, the transcript abundance of the downstream genes was analyzed in AFS-I-*tic22* (AFS-I) by RT-PCR and compared with the transcript abundance seen in WT. The combinations of oligonucleotides are indicated, and *rnpB* (*lanes 9* and *10*) was amplified as control. *C*, indicated strains were spotted on BG11 plates (*left*) with 30 mM lysozyme as described in *B*. For immunoblot (*bottom*), similar amounts of cells were subjected to SDS-PAGE and immunodecorated with *ana*Tic22 antibodies. *D*, identical amounts of cell lysate from indicated strains were subjected to immunodecoration by *ana*Tic22 and AtpB antibodies. *E*, same samples as in *D* were subjected to immunodecoration by *ana*Omp85 antibodies. The cell extract from *Anabaena* sp. was incubated without (*left*) or with anaOmp85-POTRA-His (*right*), immobilized on NTA. Eluted protein was subjected to SDS-PAGE followed by Coomassie Blue staining. *F*, expressed *ana*Omp85-POTRA-His (*lanes 1–3*) and *ana*Tic22-His (*lanes 3–5*) incubated with glutaraldehyde (*lanes 2–4*) was subjected to SDS-PAGE followed by Coomassie Blue staining. *ana*Omp85-POTRA (*black*), *ana*Tic22 (*white*), and POTRA-*ana*Tic22 (*gray*) cross-links are highlighted by *triangles*. *G*, *Anabaena* cells were incubated with formaldehyde, solubilized (*I, lanes 1* and *6*), and incubated with antibodies against *ana*Omp85 (*lanes 7–10*). After affinity purification, the flow-through (*F, lanes 2* and *7*), wash (*W, lanes 3, 4, 8,* and *9*), and elution fraction (*E, lanes 5* and *10*) was collected and subjected to SDS-PAGE followed by Coomassie Blue staining. The region of *lane 10* indicated (*arrowheads*) were excised, boiled, and subjected to SDS-PAGE, blotted, and immunodecorated with *ana*Tic22 antibodies (*lanes 11* and *12*). The migration of the heavy chain (*HC*) and light chain (*LC*) of the antibody (*black arrowhead*) and of *ana*Tic22 (*white arrowhead*) is indicated.

Chemical cross-linking of purified *ana*Omp85-POTRA-HIS with glutaraldehyde (Fig. 4*G, lane 2*) stabilized the previously determined dimeric conformation (*black triangle*; 16). Similarly, a dimeric form of the purified *ana*Tic22-HIS according to the migration of the cross-linked product is observed (*lane 4, white triangle*). However, the majority of both proteins was not cross-linked and migrated as monomer. Addition of the glutaraldehyde to a mixture of *ana*Tic22 and *ana*Omp85-POTRA yielded an additional cross-link product migrating between dimeric *ana*Tic22 and dimeric POTRA suggestive of an *ana*Tic22-POTRA complex (*lane 3, gray triangle*). Interestingly, in the combination of both proteins the majority of *ana*Tic22 was cross-linked.

In parallel, we probed for an interaction *in vivo* by chemical cross-linking using intact cells, followed by cell fractionation and immunoprecipitation (Fig. 4*H*). Using antibodies specific for *ana*Omp85, we observed an elution profile distinct from the control precipitation (*lane 5 versus 10*). After excising the bands from the gel and cleaving the cross-link by boiling, the proteins were immunodecorated with *ana*Tic22 antibodies. In the upper band determined by *ana*Omp85-based precipitation, we could not detect *ana*Tic22 (*lane 11*), whereas in the second band, we identified *ana*Tic22 (*lane 12*). The latter confirms that *ana*Tic22 was precipitated by *ana*Omp85 antibodies after cross-linking. However, the major band detected in the Coomassie staining was the *ana*Omp85 antibody as the heavy and light chain was stained with the secondary antibodies as well. Thus, the mass spectrometric analysis (Fig. 4*F*), the *in vitro* analysis (Fig. 4*G*), and the *in vitro* cross-linking (Fig. 4*H*) strongly support the existence of the physical interaction between *ana*Tic22 and *ana*Omp85.

anaTic22 Has Symmetric Butterfly Structure—To gain further insights into the function of Tic22, we determined the three-dimensional crystal structure of *ana*Tic22. The crystallographic structure was solved by multiple anomalous dispersion using seleno-methionine-modified protein (supplemental Table S2). *ana*Tic22 adopts a symmetric structure (Fig. 5, *A* and *B*) with two domains (*A* and *B*) of mixed αβ topology. The two domains are nearly symmetrical with the N-terminal domain comprising 122 amino acids and the C-terminal domain 104 amino acids, respectively (Fig. 5, *A* and *B*). Each domain contains a central β-sheet with five β-strands and two interspersed helices α1 and α2 (Fig. 5, *A* and *B*). Structural variations between the two subdomains are observed with respect to loop lengths, and a short helix (αB2′) is inserted in the C-terminal domain between α2 and β5. In the N-terminal domain, a short helix (αA1′) is inserted between α1 and β4 and a helix (αA0) precedes the domain at the N terminus. Helices α1 and α3 from both domains form a cross-like arrangement with all four helices oriented almost perpendicular to each other (Fig. 5*B*). The pocket at the four-helix cross provides an electrostatic potential of mixed character (Fig. 5*C*).

anaTic22 Surface Exposes Functionally Relevant Hydrophobic Pockets—A tunnel runs through the protein at the binding interface of the two subdomains, which is interrupted by a septum resulting in two funnel-like pockets. The residues forming the septum are of conserved hydrophobic character (Fig. 5*D* and supplemental Figs. S4 and S5). In addition, the *ana*Tic22
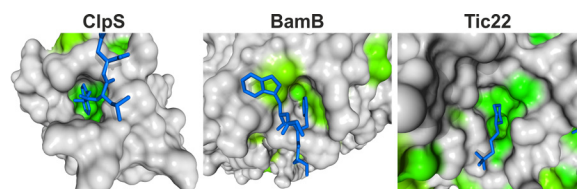
A

B

C

D

FIGURE 5. **The structure of *ana*Tic22.** *A*, the topology diagram of *ana*Tic22 is shown, indicating the general fold and its symmetry. *B*, the *ana*Tic22 structure contains two domains with a central β-sheet of five β-strands (*yellow* and *red*) and helices α1 (*light green*), α2 (*turquoise*), and α3 (*blue*). Elements of domain A and unique elements in domain B are labeled. *C*, surface representation, rotated by 90° with respect to *A* shows the electrostatic potential of the solvent accessible surface (kJ/mol) of *ana*Tic22 calculated considering implicit solvent and counter ions (54). *D*, the average hydrophobicity (55) of each column in the alignment of cyanobacterial Tic22 proteins (supplemental Table S3) is shown on the molecular surface with coloring from 4.5 (Ile, *dark green*) to −0.4 (Gly, *yellow*), and positions more hydrophilic (<−0.4; *gray*). Solvent molecules are shown as *sticks*.

structure shows several distinct hydrophobic and conserved surface pockets and patches (Fig. 5*D* and supplemental Fig. S6). Interestingly, the hydrophobic "path" surrounding the *ana*Tic22 structure is comparable with the substrate binding cleft of the tetrameric SecB, a cytosolic chaperone recognizing a broad signature enriched in aromatic and basic residues (37–39). Similarly, the periplasmic chaperone SurA from *E. coli* contains a hydrophobic surface optimized to bind sequences enriched in aromatic residues (40).

Two of the identified hydrophobic pockets (Fig. 5*D*, pockets 2 and 4) are occupied by zwitterionic buffer compounds with a

A

B

C

FIGURE 6. **Conserved functional pockets of *ana*Tic22.** *A*, surface representation of *ana*Tic22 with coloring of elements conserved in plants and cyanobacteria (min 70%; supplemental Fig. S6). The proposed influence of point mutations is shown for regions framed by replacing the according amino acids. *B*, CSR10, I-*tic22*, and I-*tic22* transformed with *anatic22* variants were grown in BG11 and proteins immunodecorated with indicated antibodies. *C*, 2 μl of the strains (2.5 mg chlorophyll ml⁻¹) were spotted on BG11 plates (*lane 1*) containing 30 mM lysozyme (*lane 2*) and grown for 7 days.

hydrophobic cyclohexyl ring. These occupancies correlate with the dependence on the presence of CAPS or CHES buffer in the formulation for successful crystallization. The electron density observed in pocket 2 could be unambiguously fitted with a cyclohexyl ring bound in the hydrophobic pocket, whereas the charged sulfonic acid side chain protrudes into solvent. Electron density in pocket 4 (Fig. 5*D*) shows the buffer molecule similarly positioned as in pocket 2.

Thus, we analyzed the potential functional relevance of the hydrophobic pockets by replacement of amino acid thought to manipulate the pocket properties based on simple surface inspection (Fig. 6*A*). We expressed *ana*Tic22 with aspartic acid 213 substituted by arginine (pocket 2), isoleucine 219 by arginine, and phenylalanine 136 by glycine (both pocket 3) in I-*tic22* (Fig. 6*B*). Growth of I-*tic22* complemented with *ana*Tic22_{F136G} in the presence of lysozyme is comparable with I-*tic22* petJ/*anatic22* (Fig. 6*C*), whereas the other two mutants did not complement for the loss of wild-type *ana*Tic22 (Fig. 6*C*). The observed complementation of the Phe-136 mutant is consistent with the variability at this position (supplemental Fig. S5). In contrast, the failed complementation of I-*tic22* with the other two mutants points to an important function of the surface pockets.

DISCUSSION

Importance of Cyanobacterial Tic22—The observed defect in the ultra-structure of the outer membrane observed in the mutants with dysfunctional *ana*Omp85 and *ana*Tic22 strongly suggests a function of the two proteins in the outer membrane biogenesis of *Anabaena* sp. PCC7120 (Fig. 3 and supplemental

Fig. S2). This result is consistent with the fragmentation phenotype observed for I-*alr2269* (23). Interestingly, *anatic22* is more strongly expressed in heterocysts than in vegetative cells under diazotrophic conditions as judged from the promoter GFP fusion expression (Fig. 2). In contrast, *omp85* genes do not show an enhanced expression (23), which might either be a explained by the existence of three distinct genes coding for Omp85-like proteins (23) or by an anyhow very high expression and protein content of this factor (27, 41). The enhanced expression of *anatic22* during heterocyst development parallels the observation that the insertion mutant of *anatic22* does not grow under these conditions (Fig. 3). This could suggest that heterocyst formation requires an alteration of the outer membrane proteome. However, the reorganization of the cell wall during heterocyst formation is not accompanied with significant proteome change in terms of the type of proteins (27, 41) but may with respect to the quantity of certain factors. The latter notion, however, has not been experimentally confirmed so far. However, it would be consistent with the impaired heterocyst development or function when genes are mutated, which code for secreted proteins involved in heterocyst-specific glycolipid layer and heterocyst envelope polysaccharide layer formation (summarized in Refs. 42 and 43). Thus, the outer membrane integrity appears to be central for heterocyst development, and *ana*Tic22 is an important factor thereof.

Dual Localization of Cyanobacterial Tic22—The cyanobacterial Tic22 resides in both, the periplasm and in the thylakoid system (Fig. 2) (18, 19). Previously, it was suggested that the dual localization of the protein in *Synechocystis* sp. 6803 is a result of two possible translational start points (18). Remarkably, the protein from *Anabaena* sp. does not contain the two start points (supplemental Fig. S7). However, in *Synechocystis* sp. 6803, only <5% of the Tic22 protein was assigned to the periplasm, whereas the periplasmic fraction of Tic22 in *Anabaena* sp. appears to be significantly larger (Fig. 2). Thus, we have to conclude that the localization to the thylakoids is not strictly dependent on this additional signal, at least in *Anabaena* sp.

Consistent with the previous report, we could not isolate fully segregated mutants, which suggests that the protein is essential for cyanobacterial growth in general (Fig. 3; 18). However, the photosynthetic activity was reduced in the merodiploid *Synechocystis* strain (18), whereas we report a defect comparable with the one observed for *omp85* mutants for the *Anabaena* sp. mutant (Fig. 3). In addition, we could not establish a significant defect of the photosynthetic activity or of the photosynthetic complexes (supplemental Fig. S7) (44). Whether the latter observation suggests a different functionality of Tic22 of the unicellular *Synechocystis* and of the filamentous *Anabaena* sp. has to be further investigated. Nevertheless, based on the similarity between *syn*Tic22 and *ana*Tic22 with respect to the second translation point, it is tempting to assume that the importance of *ana*Tic22 for the outer membrane biogenesis is conserved between different cyanobacteria.

Comparison between Cyanobacterial Tic22 and Proteobacterial SurA—The transfer of β-barrel proteins through the periplasm of Gram-negative bacteria is assisted by the chaperone SurA (13, 40, 45), which does not exist in cyanobacteria (4).

FIGURE 7. **Comparison of the hydrophobic surface pockets of *ana*Tic22, BamB, and ClpS.** Surface of ClpS with bound tripeptide (Trp, Leu, Phe; Protein Data Bank code 3GQ1 (47)); BamB with Trp-103 and Phe-104 of a neighboring molecule (Protein Data Bank code 3PRW) (21) and pocket 2 of *ana*Tic22 (180° rotated to C). Each amino acid is colored in *green* according to the average hydrophobicity (55) in the alignment (supplemental Table S3-S6) with a cut-off of 1.8 (alanine).

Here, we provide evidence that the periplasmic function of cyanobacterial Tic22 is linked to Omp85 (Fig. 4). The phenotype of I-*tic22* with respect to OM biogenesis is alike the one of cyanobacterial *omp85* (23) or proteobacterial *surA* or *bamB* mutants (46). Furthermore, SurA, BamB, and Tic22 interact with Omp85. However, *ana*Tic22 and SurA bind more transiently to Omp85 than BamB (Fig. 4) (3 6, 45, 46).

The structure of *ana*Tic22 further supports this notion as it contains a hydrophobic surface, a property that is often found in chaperones (Fig. 5) (39, 40). These hydrophobic patches are accompanied by functional hydrophobic surface pockets (Figs. 5 and 6) similar to those found in ClpS (Fig. 7) (47). ClpS is a substrate receptor of the *N*-end rule pathway delivering substrates to the ClpAP protease (20). The surface pocket of ClpS is involved in the recognition of the Leu, Phe, Tyr, or Trp residues of the N-terminal degrons in the clients. In addition, BamB, a protein involved in the OMP assembly (13), has a hydrophobic pocket binding to aromatic ligands (Fig. 7) as inferred from crystal contacts (21, 48–50). Consistently, a C-terminal aromatic amino acid serves as a signal for the insertion of OMPs into the OM (13).

It appears that the cyanobacterial Tic22 might have a function comparable with the proteobacterial SurA. However, SurA does only exist in proteobacteria, leaving the question whether a Tic22-like protein participates in the periplasmic transfer of OMPs in other bacteria. Remarkably, by searching for structural homologues with DALI (51), we identified only one protein of unknown function from *Thermus thermophilus* (DALI score 4.9, Protein Data Bank code 2Z0R, TTHA0547). It resembles one subdomain, however, with notable alterations (Fig. 8) (supplemental Fig. S8). The root mean square deviation over 63 Cα positions between TTHA0547 and the subdomain A of *ana*Tic22 amounts to 2.4 Å and to 3.2 Å over 70 Cα positions with subdomain B.

According to the tree of life proposed by Cavalier-Smith *T. thermophilus* branched off from the common clade before cyanobacteria (52). Thus, the observed symmetry in the structure of the cyanobacterial Tic22 and the "single domain" structure of the protein from *Thermus thermophilus* points to a gene duplication event in case of the cyanobacterial protein (Fig. 5). In addition, the proteins in hado- and cyanobacteria may have a comparable function, which suggests a unifying principle in the transport of OM proteins in bacteria, whereas the molecular nature of the periplasmic chaperone differs. Thus, it will be interesting to determine the function of the *T. thermophilus* protein in future.
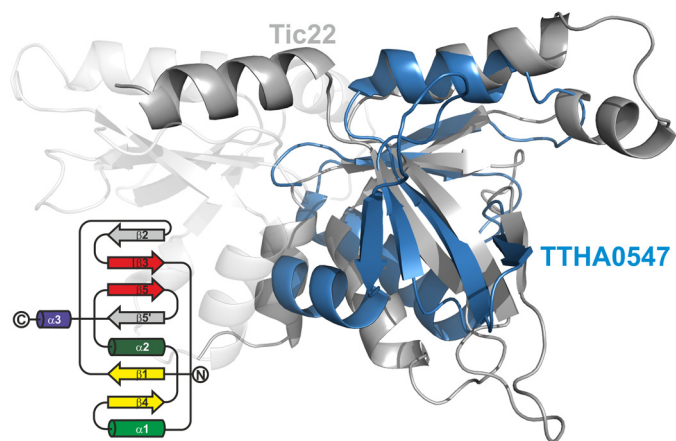
FIGURE 8. **A structural homologue in *T. thermophilus*.** The overlay of the structure of TTHA0547 (*blue*) and *ana*Tic22 (*gray*) is shown. The topology diagram of TTHA0547 is shown on the *left*.

Eukaryotic Tic22 Is Inherited from Cyanobacteria—Our understanding of protein translocation across the intermembrane space of chloroplasts is sparse. Tic22 is so far the only discovered soluble intermembrane space translocon component (6, 7). The related cyanobacterial protein (Fig. 1 and supplemental Fig. S1) is distributed to both periplasm and thylakoids (Fig. 1) (18, 19), and the periplasmic localization of Tic22 appears to be evolutionarily conserved (8–10). Evidence for a functional conservation is provided by the observed complementation of the outer membrane biogenesis phenotype of the *anatic22* mutant by the plant protein (Fig. 4). Similar to the proposed functional analogy between cyanobacterial Tic22 and SurA or BamB in proteobacteria, the plant Tic22 could fulfill a function comparable with the tiny Tims in the intermembrane space of mitochondria (5, 6).

Tic22 represents the second chloroplast translocation component besides Toc75 (53), for which a phylogenetic and functional relationship to the cyanobacterial homologue can be established. All other translocon components are rather products of an evolutionary "recycling" of proteins with functions distinct from protein translocation, or eukaryotic inventions (Fig. 1). Thus, although the directionality of the translocation path in plastids has been inverted, the minimal module composed of Omp85 and Tic22 is evolutionarily conserved.

REFERENCES

1. Cavalier-Smith, T. (2006) Origin of mitochondria by intracellular enslavement of a photosynthetic purple bacterium. *Proc. Biol. Sci.* **273**, 1943–1952
2. Archibald, J. M. (2009) The puzzle of plastid evolution. *Curr. Biol.* **19**, R81-R88
3. Alcock, F., Clements, A., Webb, C., and Lithgow, T. (2010) Evolution. Tinkering inside the organelle. *Science.* **327**, 649–650
4. Bohnsack, M. T., and Schleiff, E. (2010) The evolution of protein targeting and translocation systems. *Biochim. Biophys. Acta* **1803,** 1115–1130
5. Chacinska, A., Koehler, C. M., Milenkovic, D., Lithgow, T., and Pfanner, N. (2009) Importing mitochondrial proteins: Machineries and mechanisms. *Cell* **138,** 628–644
6. Schleiff, E., and Becker, T. (2011) Common ground for protein translocation: Access control for mitochondria and chloroplasts. *Nat. Rev. Mol. Cell Biol.* **12,** 48–59
7. Kessler, F., and Schnell, D. (2009) Chloroplast biogenesis: Diversity and regulation of the protein import apparatus. *Curr. Opin. Cell Biol.* **21,** 494–500
8. Kouranov, A., and Schnell, D. J. (1997) Analysis of the interactions of preproteins with the import machinery over the course of protein import into chloroplasts. *J. Cell Biol.* **139,** 1677–1685
9. Kouranov, A., Chen, X., Fuks, B., and Schnell, D. J. (1998) Tic20 and Tic22 are new components of the protein import apparatus at the chloroplast inner envelope membrane. *J. Cell Biol.* **143,** 991–1002
10. Becker, T., Hritz, J., Vogel, M., Caliebe, A., Bukau, B., Soll, J., and Schleiff, E. (2004) Toc12, a novel subunit of the intermembrane space preprotein translocon of chloroplasts. *Mol. Biol. Cell* **15,** 5130–5144
11. Kalanon, M., and McFadden, G. I. (2008) The chloroplast protein translocation complexes of *Chlamydomonas reinhardtii*: A bioinformatic comparison of Toc and Tic components in plants, green algae, and red algae. *Genetics.* **179,** 95–112
12. Hewitt, V., Alcock, F., and Lithgow, T. (2011) Minor modifications and major adaptations: The evolution of molecular machines driving mitochondrial protein import. *Biochim. Biophys. Acta* **1808,** 947–954
13. Knowles, T. J., Scott-Tucker, A., Overduin, M., and Henderson, I. R. (2009) Membrane protein architects: The role of the BAM complex in outer membrane protein assembly. *Nat. Rev. Microbiol.* **7,** 206–214
14. Schleiff, E., Maier, U. G., and Becker, T. (2011) Omp85 in eukaryotic systems: One protein family with distinct functions. *Biol. Chem.* **392,** 21–27
15. Jacob-Dubuisson, F., Villeret, V., Clantin, B., Delattre, A. S., and Saint, N. (2009) First structural insights into the TpsB/Omp85 superfamily. *Biol. Chem.* **390,** 675–684
16. Ertel, F., Mirus, O., Bredemeier, R., Moslavac, S., Becker, T., and Schleiff, E. (2005) The evolutionarily related beta-barrel polypeptide transporters from *Pisum sativum* and Nostoc PCC7120 contain two distinct functional domains. *J. Biol. Chem.* **280,** 28281–28289
17. Koenig, P., Mirus, O., Haarmann, R., Sommer, M. S., Sinning, I., Schleiff, E., and Tews, I. (2010) Conserved properties of polypeptide transport-associated (POTRA) domains derived from cyanobacterial Omp85. *J. Biol. Chem.* **285,** 18016–18024
18. Fulda, S., Norling, B., Schoor, A., and Hagemann, M. (2002) The Slr0924 protein of *Synechocystis* sp. strain PCC 6803 resembles a subunit of the chloroplast protein import complex and is mainly localized in the thylakoid lumen. *Plant Mol. Biol.* **49,** 107–118
19. Fulda, S., Mikkat, S., Schröder, W., and Hagemann, M. (1999) Isolation of salt-induced periplasmic proteins from *Synechocystis* sp. strain PCC 6803. *Arch. Microbiol.* **171,** 214–217
20. Sriram, S. M., Kim, B. Y., and Kwon, Y. T. (2011) The *N*-end rule pathway: Emerging functions and molecular principles of substrate recognition. *Nat. Rev. Mol. Cell Biol.* **12,** 735–747
21. Heuck, A., Schleiffer, A., and Clausen, T. (2011) Augmenting β-augmentation: Structural basis of how BamB binds BamA and may support folding of outer membrane proteins. *J. Mol. Biol.* **406,** 659–666
22. Moslavac, S., Nicolaisen, K., Mirus, O., Al Dehni, F., Pernil, R., Flores, E., Maldener, I., and Schleiff, E. (2007) A TolC-like protein is required for heterocyst development in *Anabaena* sp. strain PCC 7120. *J. Bacteriol.* **189,** 7887–7895
23. Nicolaisen, K., Mariscal, V., Bredemeier, R., Pernil, R., Moslavac, S., López-Igual, R., Maldener, I., Herrero, A., Schleiff, E., and Flores, E. (2009) The outer membrane of a heterocyst-forming cyanobacterium is a permeability barrier for uptake of metabolites that are exchanged between cells. *Mol. Microbiol.* **74,** 58–70
24. Nicolaisen, K., Hahn, A., Valdebenito, M., Moslavac, S., Samborski, A., Maldener, I., Wilken, C., Valladares, A., Flores, E., Hantke, K., and Schleiff, E. (2010) The interplay between siderophore secretion and coupled iron

and copper transport in the heterocyst-forming cyanobacterium *Anabaena* sp. PCC 7120. *Biochim. Biophys. Acta* **1798,** 2131–2140

25. Bendtsen, J. D., Nielsen, H., von Heijne, G., and Brunak, S. (2004) Improved prediction of signal peptides: SignalP 3.0. *J. Mol. Biol.* **340,** 783–795

26. Rippka, R., Deruelles, J., Waterbury, J. B., Herdman, M., and Stanier, R. Y. (1979) Generic assignments, strain histories and properties of pure cultures of cyanobacteria. *Microbiology* **111,** 1–61

27. Moslavac, S., Bredemeier, R., Mirus, O., Granvogl, B., Eichacker, L. A., and Schleiff, E. (2005) Proteomic analysis of the outer membrane of *Anabaena* sp. strain PCC 7120. *J. Proteome. Res.* **4,** 1330–1338

28. Black, K., Buikema, W. J., and Haselkorn, R. (1995) The hglK gene is required for localization of heterocyst-specific glycolipids in the cyanobacterium *Anabaena* sp. strain PCC 7120. *J. Bacteriol.* **177,** 6440–6448

29. Van Duyne, G. D., Standaert, R. F., Karplus, P. A., Schreiber, S. L., and Clardy, J. (1993) Atomic structures of the human immunophilin FKBP-12 complexes with FK506 and rapamycin. *J. Mol. Biol.* **229,** 105–124

30. Terwilliger, T. C., and Berendzen, J. (1999) Automated MAD and MIR structure solution. *Acta Crystallogr. D* **55,** 849–861

31. Emsley, P., and Cowtan, K. (2004) Coot: Model-building tools for molecular graphics. *Acta Crystallogr. D* **60,** 2126–2132

32. Murshudov, G. N., Vagin, A. A., Dodson, E. J. (1997) Refinement of macromolecular structures by the maximum-likelihood method. *Acta Crystallogr. D* **53,** 240–255

33. Lamzin, V. S., and Wilson, K. S. (1999) Automated refinement for protein crystallography. *Methods Enzymol.* **276,** 269–305

34. Laskowski, R. A., MacArthur, M. W., Moss, D. S., and Thornton, J. M. (1993) PROCHECK: A program to check the stereochemical quality of protein structures. *J. Appl. Cryst.* **26,** 283–291

35. Pernil, R., Picossi, S., Mariscal, V., Herrero, A., and Flores, E. (2008) ABC-type amino acid uptake transporters Bgt and N-II of *Anabaena* sp. strain PCC 7120 share an ATPase subunit and are expressed in vegetative cells and heterocysts. *Mol. Microbiol.* **67,** 1067–1080

36. Sklar, J. G., Wu, T., Kahne, D., and Silhavy, T. J. (2007) Defining the roles of the periplasmic chaperones SurA, Skp, and DegP in *Escherichia coli.* *Genes Dev.* **21,** 2473–2484

37. Knoblauch, N. T., Rüdiger, S., Schönfeld, H. J., Driessen, A. J., Schneider-Mergener, J., and Bukau, B. (1999) Substrate specificity of the SecB chaperone. *J. Biol. Chem.* **274,** 34219–34225

38. Dekker, C., de Kruijff, B., and Gros, P. (2003) Crystal structure of SecB from *Escherichia coli.* *J. Struct. Biol.* **144,** 313–319

39. Bechtluft, P., Nouwen, N., Tans, S. J., Driessen, A. J. (2010) SecB–a chaperone dedicated to protein translocation. *Mol. Biosyst* **6,** 620–627

40. Xu, X., Wang, S., Hu, Y. X., and McKay, D. B. (2007) The periplasmic bacterial molecular chaperone SurA adapts its structure to bind peptides in different conformations to assert a sequence preference for aromatic residues. *J. Mol. Biol.* **373,** 367–381

41. Moslavac, S., Reisinger, V., Berg M., Mirus, O., Vosyka, O., Plöscher, M.,

Flores, E., Eichacker, L. A., and Schleiff, E. (2007) The proteome of the heterocyst cell wall in *Anabaena* sp. PCC 7120. *Biol. Chem.* **388,** 823–829

42. Nicolaisen, K., Hahn, A., and Schleiff, E. (2009) The cell wall in heterocyst formation by *Anabaena* sp. PCC 7120. *J. Basic Microbiol.* **49,** 5–24

43. Flores, E., and Herrero, A. (2010) Compartmentalized function through cell differentiation in filamentous cyanobacteria. *Nat. Rev. Microbiol.* **8,** 39–50

44. Ladig, R., Sommer, M. S., Hahn, A., Leisegang, M. S., Papasotiriou, D. G., Ibrahim, M., Elkehal, R., Karas, M., Zickermann, V., Gutensohn, M., Brandt, U., Klösgen, R. B., Schleiff, E. (2011) A high-definition native polyacrylamide gel electrophoresis system for the analysis of membrane complexes. *Plant J.* **67,** 181–194

45. Ieva, R., Tian, P., Peterson, J. H., and Bernstein, H. D. (2011) Sequential and spatially restricted interactions of assembly factors with an autotransporter β domain. *Proc. Natl. Acad. Sci. U.S.A.* **108,** E383–391

46. Vuong, P., Bennion, D., Mantei, J., Frost, D., and Misra, R. (2008) Analysis of YfgL and YaeT interactions through bioinformatics, mutagenesis, and biochemistry. *J. Bacteriol.* **190,** 1507–1517

47. Román-Hernández, G., Grant, R. A., Sauer, R. T., and Baker, T. A. (2009) Molecular basis of substrate selection by the *N*-end rule adaptor protein ClpS. *Proc. Natl. Acad. Sci. U.S.A.* **106,** 8888–8893

48. Kim, K. H., and Paetzel, M. (2011) Crystal structure of *Escherichia coli* BamB, a lipoprotein component of the β-barrel assembly machinery complex. *J. Mol. Biol.* **406,** 667–678

49. Noinaj, N., Fairman, J. W., and Buchanan, S. K. (2011) The crystal structure of BamB suggests interactions with BamA and its role within the BAM complex. *J. Mol. Biol.* **407,** 248–260

50. Albrecht, R., and Zeth, K. (2011) Structural basis of outer membrane protein biogenesis in bacteria. *J. Biol. Chem.* **286,** 27792–27803

51. Holm, L., and Rosenström, P. (2010) Dali server: Conservation mapping in three dimensions. *Nucleic Acids Res.* **38,** W545–549

52. Cavalier-Smith, T. (2006) Rooting the tree of life by transition analyses. *Biol. Direct.* **1,** 19

53. Bredemeier, R., Schlegel, T., Ertel, F., Vojta, A., Borissenko, L., Bohnsack, M. T., Groll, M., von Haeseler, A., and Schleiff, E. (2007) Functional and phylogenetic properties of the pore-forming β-barrel transporters of the Omp85 family. *J. Biol. Chem.* **282,** 1882–1890

54. Baker, N. A., Sept, D., Joseph, S., Holst, M. J., and McCammon, J. A. (2001) Electrostatics of nanosystems: Application to microtubules and the ribosome. *Proc. Natl. Acad. Sci. U.S.A.* **98,** 10037–10041

55. Kyte, J., and Doolittle, R. F. (1982) A simple method for displaying the hydropathic character of a protein. *J. Mol. Biol.* **157,** 105–132

56. Olmedo-Verd, E., Muro-Pastor, A. M., Flores, E., and Herrero, A. (2006) Localized induction of the ntcA regulatory gene in developing heterocysts of *Anabaena* sp. strain PCC 7120. *J. Bacteriol.* **188,** 6694–6699

57. Black, T. A., Cai, Y., and Wolk, C. P. (1993) Spatial expression and autoregulation of hetR, a gene involved in the control of heterocyst development in *Anabaena. Mol. Microbiol.* **9,** 77–84